processes

MDPI

*Article*

# Research on High-Pressure Hydrogen Pre-Cooling Based on CFD Technology in Fast Filling Process

**Sen Li [1,2,3], Jinxing Guo [4], Xin Lv [1,2,3], Teng Deng [1,2,3], Bo Cao [1,2,3] and Juan Wang [1,2,3,*]**

1 School of Mechanical & Electrical Engineering, Xi'an University of Architecture and Technology, Xi'an 710055, China; xauatsenli@163.com (S.L.); lvxinALZN123@163.com (X.L.); dengteng2021@126.com (T.D.); xauatbocao@163.com (B.C.)
2 Shaanxi Key Laboratory of Nanomaterials and Nanotechnology, Xi'an University of Architecture and Technology, Xi'an 710055, China
3 Xi'an Key Laboratory of Clean Energy, Xi'an University of Architecture and Technology, Xi'an 710055, China
4 Xi'an Aerospace Propulsion Institute, Xi'an 710100, China; guomalevenus@163.com
* Correspondence: juanwang@xauat.edu.cn

**Abstract:** In the fast filling process, in order to control the temperature of the vehicle-mounted storage tank not to exceed the upper limit of 85 °C, it is an effective method to add a hydrogen pre-cooling system upstream of the hydrogenation machine. In this paper, Fluent is used to simulate the heat transfer process of high-pressure hydrogen in a shell-and-tube heat exchanger and the phase change process of refrigerant R23. The accuracy of the model is proven by a comparison with the data in the references. Using this model, the temperature field and gas volume fraction in the heat transfer process are obtained, which is helpful to analyze the heat transfer mechanism. At the same time, the influence of hydrogen inlet temperature, hydrogen inlet pressure, and refrigerant flow rate on the refrigeration performance was studied. The current work shows that the model can be used to determine the best working parameters in the pre-cooling process and reduce the operating cost of the hydrogen refueling station.

**Keywords:** hydrogen refueling station; hydrogen pre-cooling system; computational fluid dynamics (CFD); shell and tube heat exchanger

check for updates

**Citation:** Li, S.; Guo, J.; Lv, X.; Deng, T.; Cao, B.; Wang, J. Research on High-Pressure Hydrogen Pre-Cooling Based on CFD Technology in Fast Filling Process. *Processes* **2021**, *9*, 2208. https://doi.org/10.3390/pr9122208

Academic Editor: Alfredo Iranzo

Received: 30 October 2021
Accepted: 26 November 2021
Published: 8 December 2021

**Publisher's Note:** MDPI stays neutral with regard to jurisdictional claims in published maps and institutional affiliations.

**Copyright:** © 2021 by the authors. Licensee MDPI, Basel, Switzerland. This article is an open access article distributed under the terms and conditions of the Creative Commons Attribution (CC BY) license (https://creativecommons.org/licenses/by/4.0/).

## 1. Introduction

Hydrogen energy is a potentially clean energy with high energy density and is pollution-free [1–3]. As a secondary energy source, hydrogen can be obtained directly from fossil raw materials, or it can be produced by electrolyzing water from renewable energy sources (such as solar energy, wind energy, etc.) [2,3]. The development of a hydrogen energy economy can reduce the emission of greenhouse gases and small particle pollutants, and at the same time achieve energy diversification. It is a potential substitute for ordinary fossil energy carriers [4]. Therefore, various countries around the world have regarded hydrogen energy as the strategic development direction of new energy source in the future.

In the field of transportation, hydrogen fuel cell vehicles have received widespread attention in recent years. Due to the high cost of acquiring and using liquid hydrogen, the current hydrogen storage methods used in hydrogen fuel cell vehicles utilize gaseous hydrogen storage. Hydrogen is the smallest known gas in the world, as the density of hydrogen is only 1/14 that of air, namely at one standard atmospheric pressure and 0 °C, hydrogen density is 0.089 g/L. To improve the cruising range of fuel cell vehicles, it is necessary to increase the storage pressure in the onboard storage tank [5,6]. At the same time, more than 80% of hydrogen refueling stations use high-pressure gaseous hydrogen storage [7]. To improve the competitiveness of hydrogen fuel cell vehicles, the filling process needs to be completed within 3–5 min [8,9]. However, in the process of rapid filling, the temperature of the storage tank rises rapidly as the pressure of the onboard

storage tank rises. The increase in tank temperature is mainly caused by the following three main thermodynamic phenomena [10]. First of all, the kinetic energy of the fast-flowing hydrogen converted into internal energy gas generates a lot of heat during the filling process. Secondly, the hydrogen expanded through the throttle valve causes the temperature to rise, which is called the Joule–Thomson effect. Third, the compression of hydrogen during the filling process of the storage tank will also cause the temperature to rise, and the increase in temperature not only reduces the storage capacity of the hydrogen tank, but may also bring potential safety hazards. Therefore, it is necessary to adopt appropriate means to control the temperature not to exceed the limit.

To ensure safety during the rapid filling process, the SAE J2601 filling agreement stipulates that the temperature of hydrogen in the onboard storage tank during the rapid filling process cannot exceed 85 °C [11,12]. There are two main reasons for setting the upper-temperature limit of 85 °C: The first is to protect the tank material from thermal degradation, and the second is to be able to fill the storage tank to the maximum without exceeding the maximum working pressure (125% of the nominal working pressure). In the research of Ortiz et al. [13], it is shown that the inlet temperature of hydrogen plays a vital role in the increase of the temperature of the vehicle-mounted storage tank during the rapid filling process. The hydrogen pre-cooling system is the most effective way to control the temperature of hydrogen [14].

Among various heat exchangers, the shell-and-tube heat exchanger (STHX) has the advantages of a reliable structure, mature technology, and wide application range, and it has been widely used in various industries [15–18]. The shell and tube heat exchanger is a very important part of the pre-cooling system, and its working parameters directly affect the effect of hydrogen pre-cooling. At the same time, in the heat exchange process of the shell-and-tube heat exchanger, the refrigerant R23 has phase change heat transfer and two-phase flow problems, which has a vital impact on the heat transfer efficiency and service life of the heat exchanger itself. With the development of computer technology, more and more numerical simulation techniques are applied to the heat transfer research of heat exchangers. Compared with experimental research methods, numerical simulation methods better facilitate the simulation of more complex or ideal working conditions. The software can obtain the fluid flow distribution field, temperature field, and velocity vector field, etc., which makes the research on the heat exchanger and its heat transfer clearer, more convenient, and faster [19]. Therefore, the effective and reasonable use of numerical simulation research will help promote the further development of heat exchanger flow and heat transfer research.

In the past, research on heat exchangers mainly focused on the study of single-phase flow, while there are few studies on the two-phase flow and heat transfer of the fluid medium in the presence of phase change heat transfer. This paper aims at analyzing the phase change heat transfer and two-phase flow through numerical simulation in the heat exchange process of high-pressure hydrogen in the shell-and-tube heat exchanger. The phase change process of refrigerant R23 was simulated using the evaporation and condensation model of the commercial fluid mechanics software Fluent 19.0 [20].

In this study, a simplified two-dimensional model of a shell-and-tube heat exchanger was simulated using CFD technology. After the grid is divided, the appropriate turbulence model and discretization scheme are selected, before the simulation is carried out by changing the hydrogen inlet temperature, the hydrogen inlet pressure, and the flow rate of the refrigerant. Through the cloud diagram and numerical curve obtained by simulation, the influence of working parameters on the pre-cooling effect is explained in detail. This provides a certain reference for selecting suitable working parameters when the pre-cooling system of the hydrogen refueling station is running and reducing the operating cost of the hydrogen refueling station.

## 2. Modeling Details

For large-scale hydrogen refueling stations that require high refueling capacity, the heat exchanger in the hydrogen pre-cooling system is a shell-and-tube heat exchanger. The diagram of the pre-cooling system of the hydrogen refueling station is shown in Figure 1. Because the cascade refrigeration system can meet the cooling requirements of −30 °C~−55 °C [21], combined with the research of Sun et al. [22], R404 a is selected as the high-temperature refrigerant, and R23 is selected as the low-temperature refrigerant in the low-temperature cycle. The shell-and-tube heat exchanger in the low-temperature system is a heat exchange device for high-pressure hydrogen and refrigerant R23. Therefore, the main content of this paper addresses the heat exchange process of the shell-and-tube heat exchanger during operation.

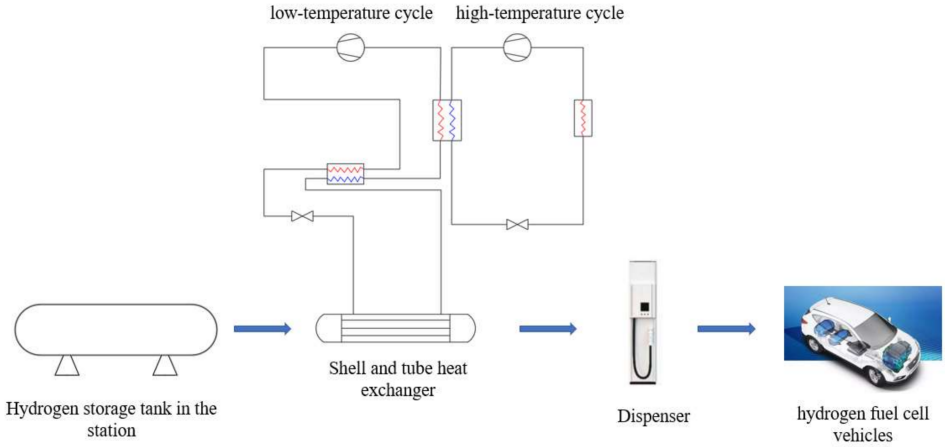


**Figure 1.** Schematic diagram of hydrogen pre-cooling system in hydrogen refueling station.

The basic principle of the shell and tube heat exchanger is that two fluids flow at different temperatures, separated by the heat exchange tube wall. According to the second law of thermodynamics, there is a temperature difference between the two fluids. Heat is transferred from the fluid with a higher temperature to the fluid with a lower temperature. The heat transfer is achieved through heat conduction and convection heat transfer mechanisms. The heat transfer principle is shown in Figure 2. Figure 2 shows the temperature change of the hot and cold fluid during the heat exchange process. $t_1'$ and $t_1''$ represent the inlet and outlet temperature of the hot fluid, and $t_2'$ and $t_2''$ represent the inlet and outlet temperature of the cold fluid.

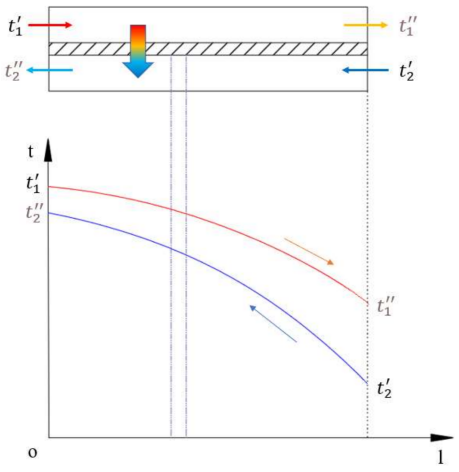


**Figure 2.** Heat transfer principle of shell and tube heat exchanger.

Due to the large difference between the outlet temperature and the inlet temperature of high-pressure hydrogen, if a multi-process shell and tube heat exchanger is used, the high-temperature gas at the inlet will exchange heat with the cooled gas, causing unnecessary cold energy loss. Therefore, this model uses a single-process shell-and-tube heat exchanger in which high-pressure hydrogen flows on the tube side and the refrigerant R23 flows on the shell side. In the heat exchange process, the shell side flow, that is, the flow of refrigerant R23 has a transition from the liquid phase to the gas phase. The commonly used single-curved baffle is shown in Figure 3a. The refrigerant R23 undergoes a phase change when heated, and the gas phase will gather in the area indicated by the arrow in the figure, which reduces the heat transfer performance of the heat exchanger. This article uses the flower (mentioned in [23,24]) type baffle to improve the heat exchange performance in the heat exchange process, as shown in Figure 3b. The material of the heat exchange tube and the shell is 316 L stainless steel. According to the actual working conditions in the heat exchange process, the average temperature difference method is used to design the heat exchanger. The geometric parameters are shown in Table 1. The three-dimensional model of the shell and tube heat exchanger is shown in Figure 4.

(**a**) (**b**)

**Figure 3.** Single-curved baffle and flower baffle in shell and tube heat exchanger. (**a**) Single-curved baffle, (**b**) flower baffle.

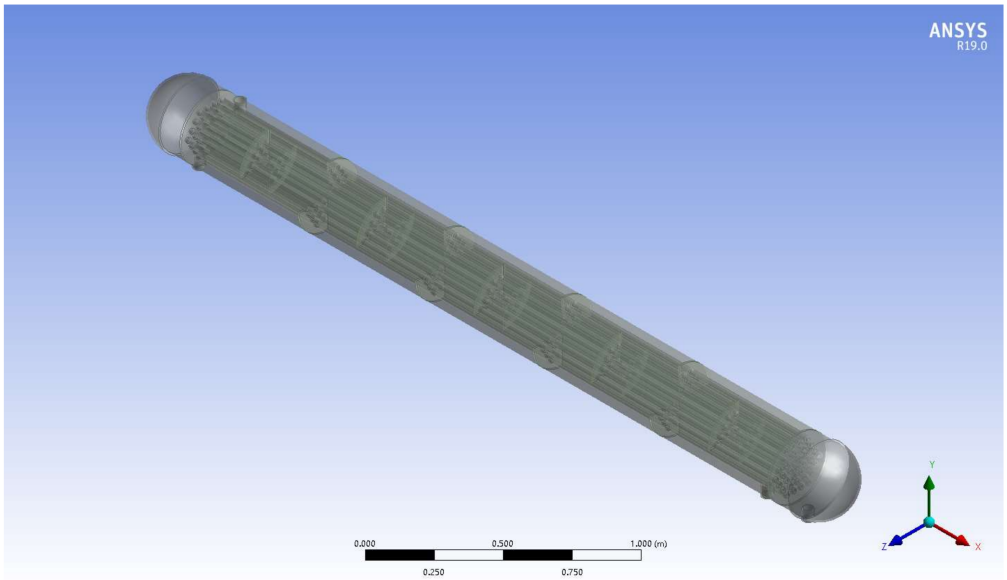


**Figure 4.** Three-dimensional model of shell-and-tube heat exchanger.

**Table 1.** Geometric parameters of the heat exchanger.

| Parameter | Value |
|---|---|
| Length (m) | 3.000 |
| Shell inside diameter (m) | 0.300 |
| Number of tubes | 31 |
| Tube outside diameter (mm) | 25 |
| Tube pitch (mm) | 37 |
| Tube thickness (mm) | 2.500 |
| Tube layout | Triangular arrangement |
| Baffle form | Flower shape |
| Number of baffles | 9 |
| Spacing of baffles (mm) | 300 |
| Number of holes on baffle | 14 |
| Shell and tube type | BEM |

### *2.1. Two-Dimensional Axisymmetric Model Establishment and Meshing*

The physical model is directly established according to the designed heat exchanger parameters, the number of elements reaches tens of millions, the calculation cycle is long, and the requirements for the computer are relatively high. In the hydrogen pre-cooling process, high-pressure hydrogen flows in the heat exchange tube, R23 flows outside the tube, and the cold and hot fluids exchange heat through the tube wall. The two-dimensional axisymmetric model can well simulate the flow of hot and cold fluids and the heat transfer process during flow. Therefore, to facilitate the calculation, the physical model of the heat exchanger is simplified to a two-dimensional axisymmetric model, as shown in Figure 5. In addition, the reason for removing the baffle is that the addition of the baffle to the two-dimensional axisymmetric model will block the flow of refrigerants.

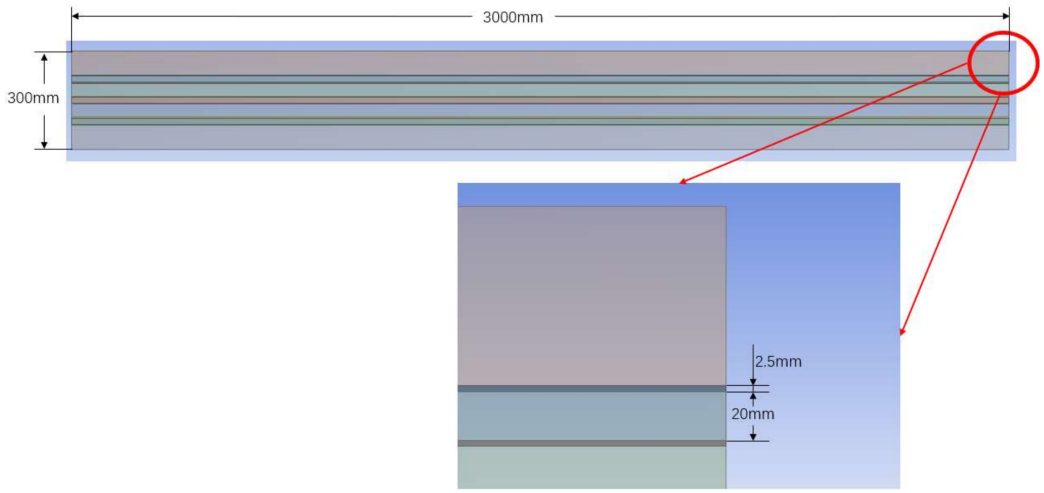


**Figure 5.** Two-dimensional axisymmetric model of the heat exchanger.

The two-dimensional axisymmetric model of the shell-and-tube heat exchanger consists of three regions. The pipeline flow area is a high-pressure hydrogen flow area. The shell side basin is the basin of refrigerant R23. The tube wall is located between the two to exchange heat between hot and cold fluids.

Due to the regular geometric shape and good symmetry of the research object, the mesh function is used to divide the two-dimensional axisymmetric structure grid, and at the same time, the grid is refined near the wall of the heat exchange tube, so that it is enough to capture the evaporation near the wall [25]. To calculate the accuracy, the grid size of the area near the heat exchange tube is set to 0.1 mm, and the grid size of the other areas is set to 2.5 mm. The total number of grids is 282,036. The details of the grid are shown in Figure 6.

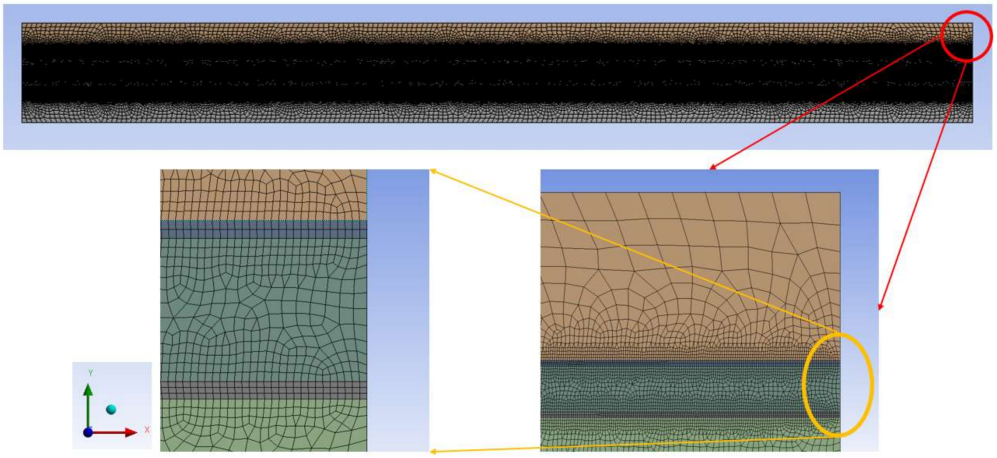

**Figure 6.** Meshing of 2D axisymmetric models.

### *2.2. Basic Assumptions*

By solving a series of control equations applied to the micro-control unit, the computational fluid dynamics method can obtain the detailed distribution of the temperature field and various volume fractions, which is helpful to analyze the heat and mass transfer behavior.

According to the heat transfer principle, a theoretical model is established. In the fluid dynamics simulation calculation, the following assumptions are made to simplify the analysis.

- Working fluid is continuous.
- Radiation heat transfer is negligible.
- The density satisfies Boussinesq approximation [26].
- Phase change materials meet the assumptions of homogeneity and isotropy.
- The liquid phase change material is a Newtonian fluid.

### *2.3. Governing Equation*

The physical model of the heat exchanger was developed in the commercial computational fluid dynamics software Ansys Fluent 19.0. Together with the control equations described below, it forms the mathematical model of the shell-and-tube heat exchanger.

Mass conservation equation:

$$\frac{\partial \rho}{\partial t} + \nabla \cdot (\rho u) = 0 \tag{1}$$

Momentum conservation equation:

$$\frac{\partial}{\partial t}(\rho u) + \nabla \cdot (\rho u) = -\nabla \cdot p + \nabla \left[ \mu \left( \nabla u + \nabla u^T - \frac{2}{3} \mu \nabla \cdot u I \right) \right] + \rho g + F_s \tag{2}$$

where: $\rho = \varphi_l \rho_l + \varphi_v \rho_v$, $\mu = \varphi_l \mu_l + \varphi_v \mu_v$, $\mathrm{FS} = 2\sigma_{l,v} \times \frac{\varphi_l \rho_l c_v \nabla \varphi_v + \varphi_v \rho_v c_l \nabla \varphi_l}{\rho_l + \rho_v}$.

Energy conservation equation:

$$\frac{\partial}{\partial t}(\rho E) + \nabla \cdot \left[ u \frac{\partial}{\partial t}(\rho E) + \nabla \cdot [u(\rho E + p)] = \nabla \cdot \left( k_{eff} \nabla T \right) + S_E \right. \tag{3}$$

where: $k_{eff} = \varphi_l k_l + \varphi_v k_v$, $E = \frac{\varphi_l \rho_l E_l + \varphi_v \mathrm{E_l}}{\varphi_l \rho_l + \varphi_v \rho_v}$, $E_v = c_{P_v} \times (T - T_{sat})$, $E_l = c_{P_l} \times (T - T_{sat})$.

The heat conduction equation in the solid of the heat pipe wall:

$$\rho_{sol} c_{P_{sol}} \frac{\partial T_{sol}}{\partial t} = k_{sol} \left( \frac{\partial^2 T_{sol}}{\partial x^2} + \frac{\partial^2 T_{sol}}{\partial y^2} \right) \tag{4}$$

where $\rho$ and $\rho_{sol}$ are the two-phase mixing density and solid density, kg/m$^3$; $u$ is the speed, m/s; $\mu$ is the dynamic viscosity, Pa/s; Fs is the surface tension, N; $\sigma_{l,v}$ is the surface tension coefficient, N/m; $c_v$ and $c_l$ are the surface curvatures; $k_{eff}$ and $k_{sol}$ are the two-phase mixed thermal conductivity and solid thermal conductivity, respectively, W/(m·K); E is the mass average internal energy, $E_v$ and $E_l$ is the internal energy of the gas and liquid phases, J; T, $T_{sat}$ and $T_{sol}$ are the two-phase mixing temperature, saturation temperature, and solid wall temperature, respectively, K; $c_{P_v}$ and $c_{P_l}$ are the specific constant pressure heat capacities of the gas and liquid phases, respectively, J/(kg·K); $c_{P_{sol}}$ is the specific heat capacity of solid at constant pressure, J/(kg·K).

### 2.4. Heat and Mass Transfer Phase Change Model

To reproduce the gas-liquid two-phase flow, the heat exchange of high-pressure hydrogen and refrigerant R23, and the phase change process of refrigerant R23 in heat exchange, the Mixture model and Lee model are used to quantitatively calculate the vapor-liquid phase change heat transfer during evaporation and condensation. The saturation temperature of R23 will change with changes in pressure, but for the stability of the calculation and the rapid convergence of the calculation results, the saturation temperature of R23 is set to 191 K. When the temperature is higher than this value, the calculation unit where the liquid phase is located will perform Evaporate. On the contrary, proceed with the condensation process.

### 2.5. Initial Conditions and Boundary Conditions

To observe the evaporation and condensation phenomenon faster, the initial temperature of R23 is set to 190.00 K, the flow rate is 0.5 m/s, the initial temperature of high-pressure hydrogen is 298.00 K, and the flow rate is 0.1 m/s. At the initial moment, the shell side fluid is all R23 liquid phase, and the tube side fluid is high-pressure hydrogen. Both the hydrogen inlet and the R23 inlet adopt the velocity inlet boundary, and the hydrogen outlet and the R23 outlet both adopt the pressure outlet boundary. Because in the actual heat exchange process, the outer layer of the heat exchanger is provided with an insulation layer to prevent the heat exchanger from exchanging heat with the external environment and reduce the loss of cooling capacity, the outer wall surface other than the inlet and outlet of the heat exchanger is set as an adiabatic boundary. The impermeable, non-slip adiabatic wall boundary conditions are used for the heat exchange tube wall. The physical parameters of the cold and hot fluid and heat exchanger materials are shown in Table 2. This paper mainly studies the phase transition and two-phase flow process of the shell side of the heat exchanger and the cooling process of the high-pressure hydrogen in the tube side. For the accuracy of the calculation, the heat exchange tube wall is treated as a constant temperature wall surface.

**Table 2.** Physical parameters of heat exchange fluid and heat exchanger materials.

| Materials | Density kg/m$^3$ | Thermal Conductivity W/(m·K) | Molar Mass g/mol |
|---|---|---|---|
| 42 MPa hydrogen | 26.9598 | 0.22 | 2.0159 |
| 47 MPa hydrogen | 29.4032 | 0.2249 | 2.0159 |
| 77 MPa hydrogen | 41.828 | 0.2563 | 2.0159 |
| R23(Liquid) | 1456 | 0.1377 | 70.01432 |
| R23(Gas) | 3.9554 | 0.00772787 | 70.01432 |
| 316 L Stainless steel | 8030 | 16.27 | / |

### 2.6. Solve Settings

The commercial code FLUENT 19.0 is adopted to simulate the flow and heat transfer in the computational model. The numerical simulation is performed with a two-dimensional transient-state turbulent flow system. The simulation time is 0–30 s, among which: the time step is 0.01 s and the number of steps is 3000 steps. The separation implicit solver is selected,

the SIMPLE algorithm based on the staggered grid is used to process the pressure-velocity coupling equation, and the first-order upwind difference format is selected to discretize the physical quantity of the control volume interface. The Mixture model is selected as the calculation model of the two-phase flow, and considered Velocity slip between phases, while the Lee model is used to simulate the transformation process of R23 from liquid phase to gas phase. The Realizable k-ε model is selected, the performance of the model is improved with mathematical constraints, the medium-strength swirling flow is predicted, and the wall-enhanced function is used to process the flow near the wall. The residual convergence standard of the continuity equation and momentum equation is $10^{-4}$, and the residual convergence standard of the energy equation is $10^{-6}$.

## 3. Model Verification

The mesh check is performed for the model. For ensuring the grid independence, the temperature of the hot fluid at the output is determined and evaluated for various meshes. Figure 7 illustrates the results of the mesh sensitivity analysis in this work. It can be seen that the output temperature of the hot liquid varies negligibly between the grid containing $2.82 \times 10^5$ and $3.24 \times 10^5$ cells. Thus, the grid with $2.82 \times 10^5$ cells is used for the simulations.

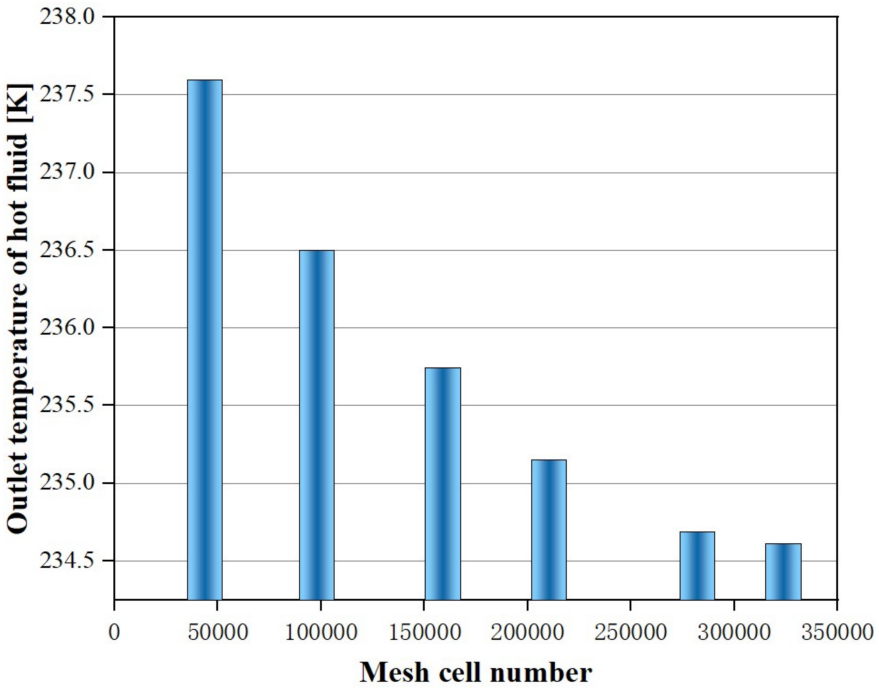


**Figure 7.** Results of the grid test for the exit temperature of the hot fluid versus the grid cell number.

To verify the feasibility of the model, the average temperature at the outlet of the shell-and-tube heat exchanger during the 77 MPa high-pressure hydrogen pre-cooling was compared with the inlet temperature of the vehicle-mounted storage tank in the fast-charging stage in the literature [27].

The hydrogen inlet temperature during the rapid filling process needs to be cooled to within −33~−40 °C within the 30 s [8], so this simulation selects the data from the previous 30 s of the simulation and references. As shown in Figure 8, the trend of the simulated temperature in this study is consistent with the data in the literature. The temperature in [27] is the inlet temperature of the vehicle-mounted storage tank during fast charging. In the refueling system of the hydrogen refueling station, the high-pressure hydrogen outlet of the shell-and-tube heat exchanger is at a distance from the hydrogen refueling machine. There is a loss of cold capacity, so the inlet temperature of the hydrogen on the vehicle storage tank is slightly higher than the outlet temperature of the hydrogen when

the simulation is completed. During the first 15 s of filling, the two temperature differences increased first and then decreased. The reason for this is that the temperature of the pipeline was still high at the beginning of the filling process. As the filling process continued, the temperature of the pipeline continued to decrease. After 15 s, the temperature difference between the two stabilized at about 5 °C. Therefore, it is appropriate to use Fluent to simulate the heat exchange process in the hydrogen pre-cooling system.

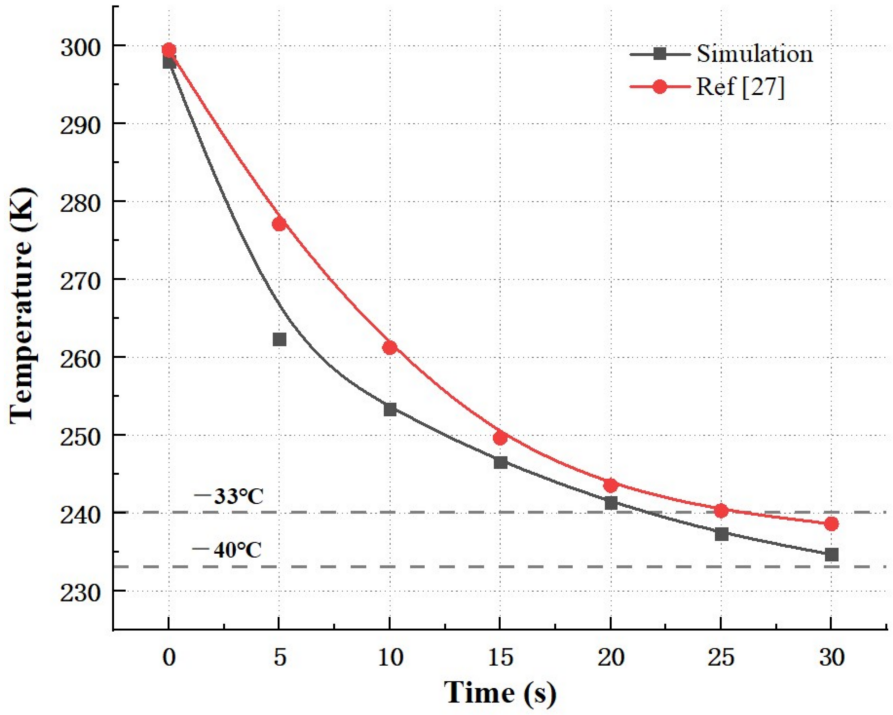


**Figure 8.** Comparison of simulation data and literature data.

## 4. Calculation Results and Discussion

After verifying the feasibility of the simulation, CFD-POST was used to visually analyze the calculation results. The influence of working parameters, such as hydrogen inlet temperature and pressure, on the pre-cooling performance is also studied.

### *4.1. Analysis of Temperature Distribution and Flow Pattern in the Heat Exchanger*

#### 4.1.1. Temperature Distribution

The hydrogen enters the heat exchange tube and exchanges heat with the refrigerant. Figure 9 shows that the temperature at the hydrogen outlet gradually decreases over time. At t = 0 s, the hydrogen temperature is the initial temperature of 298 K, and the pipe wall begins to cool the hydrogen. At t = 5 s, it can be seen that the temperature of hydrogen in the heat exchange tube has a significant drop. As time goes by, the temperature of hydrogen slowly decreases. As can be seen from Figure 6, the temperature drops to −33 °C at 22 s and the temperature drops at 30 s. There is a downward trend around −38 °C, which can meet the requirement that the temperature falls within the range of −33~−40 °C within the 30 s [8]. It can be seen from the 30 s cloud chart that the temperature in the vicinity of the high-pressure hydrogen inlet is higher, and the temperature gradient in the inlet section is larger, so the hydrogen inlet section is the area with the highest heat exchange degree of the heat exchanger.

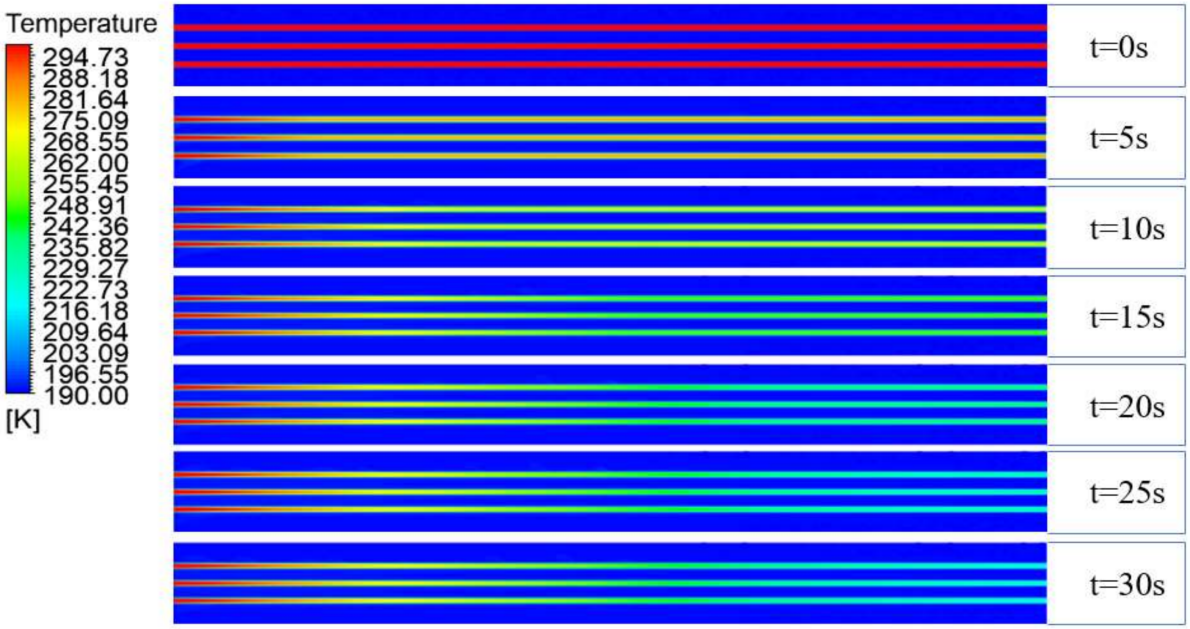


**Figure 9.** CFD simulation results in temperature cloud map.

4.1.2. Flow Pattern Analysis

In the simulation, the evaporation-condensation model was used to simulate the phase change process of the refrigerant R23, and the gas phase volume fraction cloud diagram during the simulation process and the gas phase volume fraction of the shell-side basin with time change were obtained. The value of the gas phase volume fraction in 4.2–4.4 summary is the overall gas phase volume fraction in the refrigerant flow domain. The gas-phase volume fractions of four parts of the shell-side watershed were extracted and the average value obtained was used as the gas-phase volume fraction at a certain moment. Figure 10 is the R23 vapor fraction cloud map. At t = 0 s, the shell side drainage area is dark blue, and the liquid phase occupies 100% of the shell side drainage area. It is heated by the shell side heat exchange tube wall, and the liquid phase is heated at the beginning near the wall. In the gas phase transition, as the heat exchange time increases, the proportion of the gas phase volume fraction gradually increases. From the gas phase distribution at different moments in Figure 10, it can be seen that R23 undergoes the heating phase transition of the tube wall and flows with the shell side fluid to the outlet. When t = 30 s, the gas fraction near the right side is smaller. The decrease in the dryness of R23 vapor in the final cooling phase may be due to the decrease in the temperature difference between hydrogen and R23 and the resulting decrease in flux of transferred heat and the heat transfer coefficient on the R23 side. In summary 2.5, we set the R23 outlet boundary to the pressure outlet boundary, and considering that the outlet area of the refrigerant R23 has a certain heat exchange with the outside world, the appropriate return temperature is set, which is obvious in the cold flow outlet area.

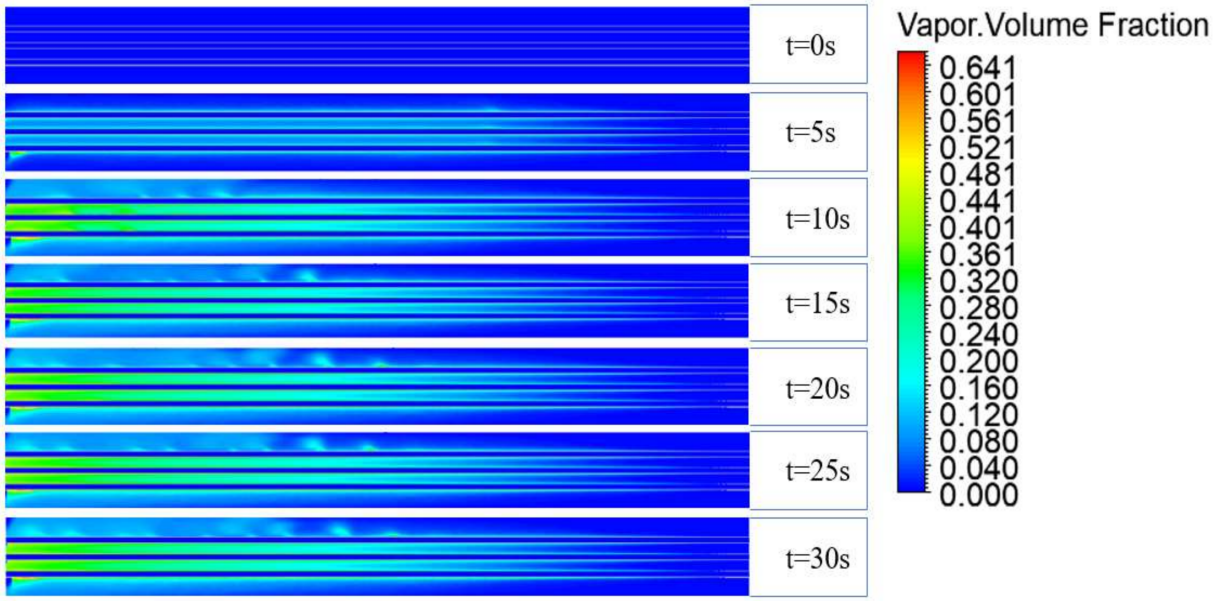


**Figure 10.** CFD simulation results in R23 gas-phase fraction cloud map.

### *4.2. The Influence of Hydrogen Inlet Pressure*

To meet different refueling requirements, hydrogen refueling stations are generally equipped with several in-station storage tanks with different pressures. The physical parameters of high-pressure hydrogen at different pressures will be different, as shown in Table 2, which will have different effects on the pre-cooling process. This study mainly analyzed the influence of pressure on the hydrogen outlet temperature during the filling process of 42 MPa, 47 MPa, and 77 MPa [2,3]. Figure 11 depicts that under different hydrogen pressures, the hydrogen outlet temperature decreases with the increase of time, and the gas volume fraction of the shell side refrigerant increases with the increase of time. It can be seen from Figure 11 that the higher the hydrogen inlet pressure, the higher the final hydrogen outlet temperature.

The maximum temperature difference between the three pressures of hydrogen during the pre-cooling process is 5.686 °C. Since the pressure of the vehicle-mounted storage tank is lower than the pressure of the storage tank in the hydrogen refueling station, in the pre-cooling system, the outlet pressure of the heat exchanger tube of the shell and tube heat exchanger is lower than the inlet pressure, and there is a certain degree of pressure drop. the pressure drop during hydrogen flow is accompanied by a temperature increase, which increases together with hydrogen pressure (Joule-Thomson effect for hydrogen). However, according to Table 2, the thermal conductivity of 77 MPa hydrogen is higher than that of 42 MPa and 47 MPa hydrogen, and the heat transfer coefficient of the entire system in the heat exchange process is higher. In summary, during the heat exchange process of 77 MPa hydrogen, the temperature is slightly higher than that of the other two pressures of hydrogen. Since the temperature difference between 42 MPa and 47 MPa hydrogen in the pre-cooling process is not very obvious, the change in the volume fraction of the gas phase reflected in the refrigerant is not very obvious.

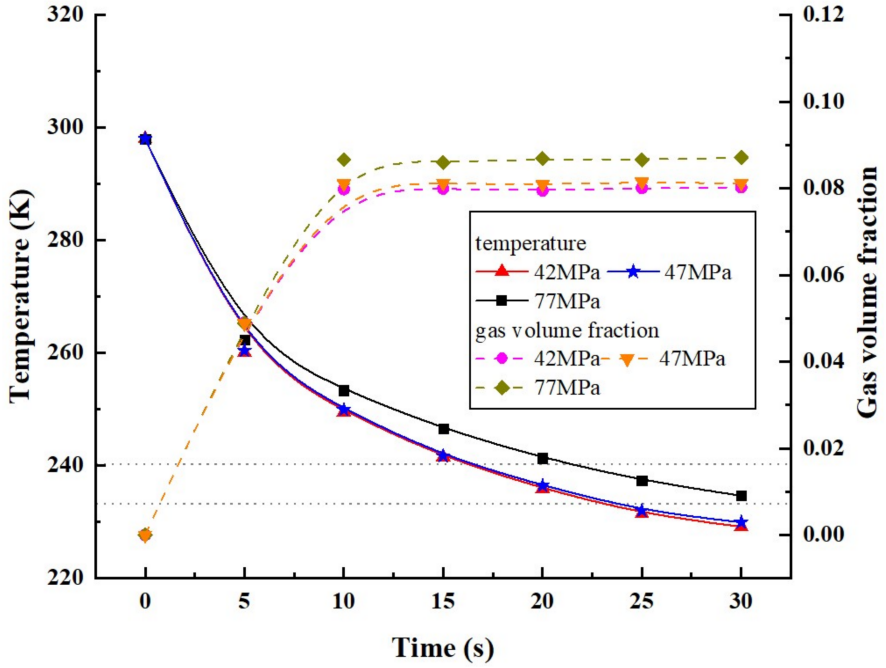


**Figure 11.** Influence of different hydrogen inlet pressures on precooling temperature and R23 gas volume fraction.

### *4.3. The Influence of Hydrogen Inlet Temperature*

The inlet temperature of hydrogen is a key factor, which largely determines the temperature of hydrogen after pre-cooling. In order to obtain the relationship between the two, the simulated pressure is 77 MPa, the hydrogen flow rate is 0.1 m/s, the refrigerant flow rate is 0.5 m/s, and the hydrogen inlet temperature is 288 K, 298 K, and 308 K, respectively. The details of the pre-cooling of different hydrogen inlet temperatures are shown in Figure 12. It can be seen that the simulation results are the same as the research results of [28], and the hydrogen outlet temperature increases with the increase of the inlet temperature. When the hydrogen inlet temperature is 288 K, the hydrogen outlet temperature will drop below −40 °C after the 20 s. At this time, other operating parameters need to be controlled so that the temperature is not too low to avoid unnecessary cooling loss. For the inlet temperature of 308 K, at the 30 s, the hydrogen outlet temperature is −33.11 °C, which barely meets the pre-cooling temperature requirements. For higher hydrogen inlet temperatures, other operating parameters need to be changed to meet the refueling requirements. In addition, in the first 15 s, the changing trend of the outlet temperature corresponding to the three different hydrogen inlet temperatures is the same. After 15 s, it can be clearly seen that the outlet temperature corresponding to the inlet temperature of 288 K hydrogen drops a little bit more. At the same time, it can be seen that a higher inlet temperature will cause a greater increase in the vapor fraction. In the first 10 s, during the pre-cooling process where the hydrogen inlet temperature is 308 K, the R23 vapor volume fraction rises the fastest. Therefore, as the temperature of high-pressure hydrogen increases, the average temperature on both sides of the cold and hot increases, the viscosity of the gas increases with the increase in temperature, and the viscosity of the refrigerant R23 decreases with the increase in temperature [28]. In the actual filling process, if the hydrogen inlet temperature is too high, the outlet temperature of the hydrogen can be reduced by increasing the flow rate of the refrigerant or reducing the flow rate of the high-pressure hydrogen to meet the filling requirements.

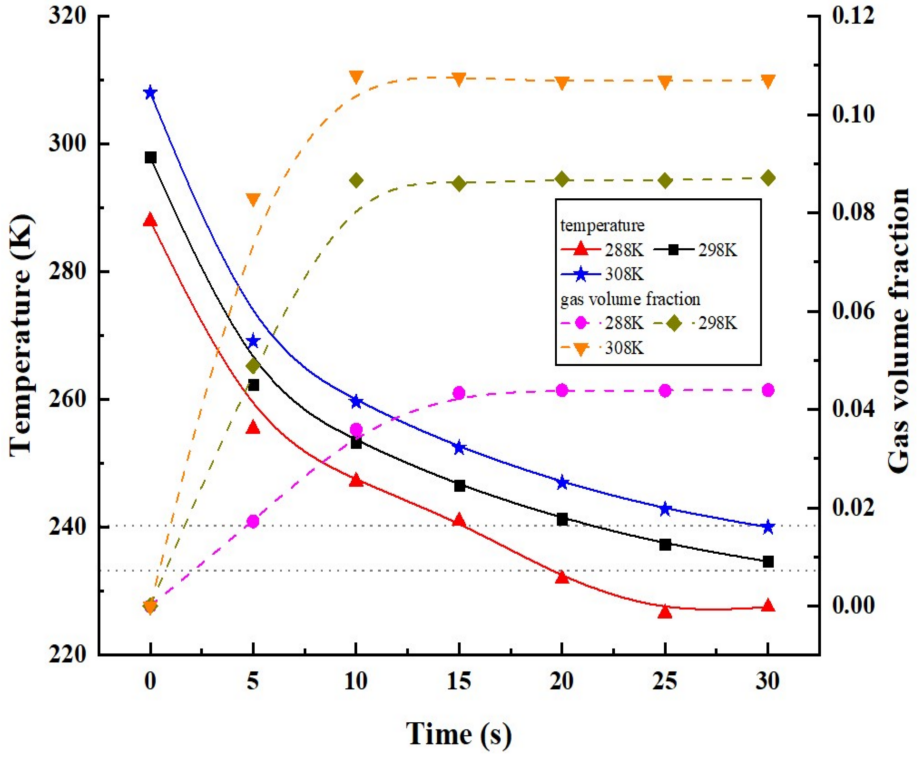


**Figure 12.** The influence of different hydrogen inlet temperatures on the pre-cooling temperature and R23 gas volume fraction.

### *4.4. Influence of Refrigerant Flow Rate*

Figure 13 shows the changes of hydrogen outlet temperature and refrigerant gas volume fraction under three different refrigerant flow rates of 0.3 m/s, 0.5 m/s, and 0.7 m/s. It can be seen from the figure that the faster the refrigerant flow rate, the better the refrigeration performance, and the greater the temperature change of the thermal fluid. The simulation results are the same as those in the literature [29]. When the refrigerant flows, the fluid is affected by the generation, floating, and flow of bubbles during the phase change of the refrigerant, causing the fluid to vortex and increase the degree of turbulence. The turbulence intensity at the inlet of the refrigerant is relatively small, and as the fluid flows along the shell side, the turbulence intensity gradually increases. When the refrigerant flow rate increases, the turbulence intensity on the shell side is significantly enhanced, which is beneficial to enhance the heat transfer effect. Since the heat transfer coefficient on the shell side is smaller than that on the tube side, the increase in the heat transfer coefficient on the shell side improves the overall heat transfer effect [30,31]. In addition, the flow rate of the refrigerant increases, the shell side fluid contacts the heat exchange tube wall more fully, the effective heat transfer area of the heat exchanger becomes larger, and the heat exchange amount of the heat exchanger also becomes larger.

It can be seen from Figure 13 that the larger the refrigerant flow rate, the smaller the volume fraction of the gas phase on the shell side. On the one hand, because the flow rate of the refrigerant increases, the gas phase is attached to the sidewall of the heat exchange tube shell and the shell side is taken out of the heat exchanger. On the other hand, the higher the refrigerant flow rate, the higher the heat transfer efficiency of the heat exchanger [28], and the lower the temperature of the shell-side tube wall, the smaller the amount of R23 that changes from liquid phase to gas phase.

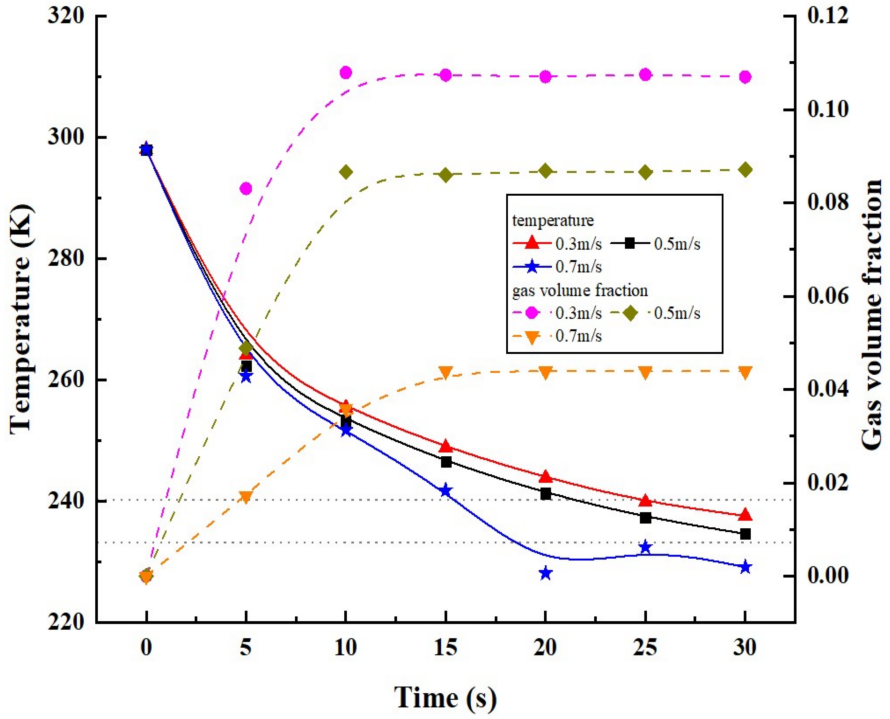


**Figure 13.** The influence of different refrigerant flow rates on pre-cooling temperature and R23 gas volume fraction.

## 5. Conclusions

In this paper, the method of computational fluid dynamics is used to simulate the heat exchange process of the shell-and-tube heat exchanger in the hydrogen pre-cooling system. Fluent software was used to simulate the cooling process of high-pressure hydrogen, the phase change heat transfer, and the two-phase flow process of R23, and the verification was carried out based on the filling data in the references. The hydrogen outlet temperature of the heat exchanger is in good agreement with the literature data. It reveals the change law of temperature field, gas volume fraction, and local heat flow in the process of liquid-phase transforming into gas-phase. According to the simulation results, the main conclusions are as follows:

- The use of CFD simulation technology can well reflect the heated phase change process, two-phase flow, and high-pressure hydrogen cooling process of R23 in the heat exchange process.
- The shell-and-tube heat exchanger for the hydrogen pre-cooling system is designed using the average temperature difference method, and the inlet temperature of the hydrogen gas during the rapid filling process is controlled to be kept within the range of −33 °C~−40 °C.
- CFD is used to simulate the heat transfer process of the shell-and-tube heat exchanger and compare it with the data in the reference. The simulation results and the experimental results have high consistency, so the simulation method is suitable for simulating the heat transfer of high-pressure hydrogen in the shell-and-tube heat exchanger.
- In the heat exchange process, the working parameters have a certain influence on the result of hydrogen pre-cooling to varying degrees. Among them, the hydrogen inlet temperature and the flow rate of the refrigerant have more obvious effects than other parameters. In the actual pre-cooling process, it is necessary to select appropriate working parameters according to the actual situation, and under the premise of ensuring safety, make the filling cost the lowest.

The results help to understand the internal flow of the tube shell heat exchanger under phase transformation heat conditions and provide appropriate working parameters for

hydrogen station in the face of different filling requirements, to reduce the operating cost of the hydrogen refueling station and promote the development of hydrogen energy.

**Author Contributions:** Conceptualization, S.L., J.G., J.W.; methodology, S.L., J.G.; software, S.L., X.L., B.C.; validation, S.L., T.D.; investigation, S.L., X.L.; writing—original draft preparation, S.L.; writing—review and editing, J.W., J.G.; funding acquisition, J.W., J.G. All authors have read and agreed to the published version of the manuscript.

**Funding:** This work was partially supported by Xi'an Key Laboratory of Clean Energy (2019219914SY S014CG036), The Yulin Industry-University-Research Cooperation Project (2019-173), and Key Research and Development Program of Shaanxi (2021ZDLGY13-02).

**Conflicts of Interest:** The authors declare no conflict of interest.

## References

1. Alazemi, J.; Andrews, J. Automotive hydrogen fuelling stations: An international review. *Renew. Sustain. Energy Rev.* **2015**, *48*, 483–499. [CrossRef]
2. Apostolou, D.; Xydis, G. A literature review on hydrogen refuelling stations and infrastructure. Current status and future prospects. *Renew. Sustain. Energy Rev.* **2019**, *113*, 109292. [CrossRef]
3. Abdalla, A.M.; Hossain, S.; Nisfindy, O.B.; Azad, A.T.; Dawood, M.; Azad, A.K. Hydrogen production, storage, transportation and key challenges with applications: A review. *Energy Convers. Manag.* **2018**, *165*, 602–627. [CrossRef]
4. Talpacci, E.; Reuβ, M.; Grube, T.; Cilibrizzi, P.; Gunnella, R.; Robinius, M.; Stolten, D. Effect of cascade storage system topology on the cooling energy consumption in fueling stations for hydrogen vehicles. *Int. J. Hydrogen Energy* **2018**, *43*, 6256–6265. [CrossRef]
5. Ahluwalia, R.K.; Hua, T.; Peng, J.K. On-board and Off-board performance of hydrogen storage options for light-duty vehicles. *Int. J. Hydrogen Energy* **2012**, *37*, 2891–2910. [CrossRef]
6. Zheng, J.; Liu, X.; Xu, P.; Liu, P.; Zhao, Y.; Yang, J. Development of high pressure gaseous hydrogen storage technologies. *Int. J. Hydrogen Energy* **2012**, *37*, 1048–1057. [CrossRef]
7. Maus, S.; Hapke, J.; Na Ranong, C.; Wüchner, E.; Friedlmeier, G.; Wenger, D. Filling procedure for vehicles with compressed hydrogen tanks. *Int. J. Hydrogen Energy* **2008**, *33*, 4612–4621. [CrossRef]
8. Elgowainy, A.; Reddi, K.; Lee, D.-Y.; Rustagi, N.; Gupta, E. Techno-economic and thermodynamic analysis of pre-cooling systems at gaseous hydrogen refueling stations. *Int. J. Hydrogen Energy* **2017**, *42*, 29067–29079. [CrossRef]
9. DOE (U.S. Department of Energy). Fuel Cell Electric Vehicles. 2016. Available online: http://www.afdc.energy.gov/vehicles/fuel_cell.html (accessed on 1 November 2021).
10. Liu, Y.-L.; Zhao, Y.-Z.; Zhao, L.; Li, X.; Chen, H.-G.; Zhang, L.-F.; Zhao, H.; Sheng, R.-H.; Xie, T.; Hu, D.-H. Experimental studies on temperature rise within a hydrogen cylinder during refueling. *Int. J. Hydrogen Energy* **2010**, *35*, 2627–2632. [CrossRef]
11. SAE. Fueling Protocols for Light Duty and Medium Duty Gaseous Hydrogen Surface Vehicles (Standard J2601-201407). 2014. Available online: http://standards.sae.org/j2601_201612/ (accessed on 3 June 2021).
12. European Commission. '2020 Climate & Energy Package' 23-Nov- Climate Action-European Commission. 2016. Available online: https://ec.europa.eu/clima/policies/strategies/2020_en (accessed on 3 March 2021).
13. Cebolla, R.O.; Acosta, B.; de Miguel, N.; Moretto, P. Effect of precooled inlet gas temperature and mass flow rate on final state of charge during hydrogen vehicle refueling. *Int. J. Hydrogen Energy* **2015**, *40*, 4698–4706. [CrossRef]
14. Li, M.; Bai, Y.; Zhang, C.; Song, Y.; Jiang, S.; Grouset, D.; Zhang, M. Review on the research of hydrogen storage system fast refueling in fuel cell vehicle. *Int. J. Hydrogen Energy* **2019**, *44*, 10677–10693. [CrossRef]
15. Wang, Y.; Liu, Z.; Huang, S.; Liu, W.; Li, W. Experimental investigation of shell-and-tube heat exchanger with a new type of baffles. *Heat Mass Transf.* **2011**, *47*, 833–839. [CrossRef]
16. Lei, Y.; Li, Y.; Jing, S.; Song, C.; Lyu, Y.; Wang, F. Design and performance analysis of the novel shell-and-tube heat exchangers with louver baffles. *Appl. Therm. Eng.* **2017**, *125*, 870–879. [CrossRef]
17. Chen, J.; Lu, X.; Wang, Q.; Zeng, M. Experimental investigation on thermal-hydraulic performance of a novel shell-and-tube heat exchanger with unilateral ladder type helical baffles. *Appl. Therm. Eng.* **2019**, *161*, 114099. [CrossRef]
18. Darbandi, M.; Abdollahpour, M.-S.; Hasanpour-Matkolaei, M. A new developed semi-full-scale approach to facilitate the CFD simulation of shell and tube heat exchangers. *Chem. Eng. Sci.* **2021**, *245*, 116836. [CrossRef]
19. Ozden, E.; Tari, I. Shell side CFD analysis of a small shell-and-tube heat exchanger. *Energy Convers. Manag.* **2010**, *51*, 1004–1014. [CrossRef]
20. ANSYS Fluent Version 19.0. Fluent 2019 User's Guide. Available online: https://ansyshelp.ansys.com/account/secured?returnurl=/Views/Secured/corp/v195/flu_ug/flu_ug.html (accessed on 10 January 2020).
21. Rezayan, O.; Behbahaninia, A. Thermoeconomic optimization and exergy analysis of $CO_2/NH_3$ cascade refrigeration systems. *Energy* **2011**, *36*, 888–895. [CrossRef]
22. Sun, Z.; Liang, Y.; Liu, S.; Ji, W.; Zang, R.; Liang, R.; Guo, Z. Comparative analysis of thermodynamic performance of a cascade refrigeration system for refrigerant couples R41/R404A and R23/R404A. *Appl. Energy* **2016**, *184*, 19–25. [CrossRef]

23. He, L.; Li, P. Numerical investigation on double tube-pass shell-and-tube heat exchangers with different baffle configurations. *Appl. Therm. Eng.* **2018**, *143*, 561–569. [CrossRef]
24. You, Y.; Fan, A.; Huang, S.; Liu, W. Numerical modeling and experimental validation of heat transfer and flow resistance on the shell side of a shell-and-tube heat exchanger with flower baffles. *Int. J. Heat Mass Transf.* **2012**, *55*, 7561–7569. [CrossRef]
25. Gu, X.; Zheng, Z.; Xiong, X.; Wang, T.; Luo, Y.; Wang, K. Characteristics of Fluid Flow and Heat Transfer in the Shell Side of the Trapezoidal-like Tilted Baffles Heat Exchanger. *J. Therm. Sci.* **2018**, *27*, 602–610. [CrossRef]
26. Gray, D.D.; Giorgini, A. The validity of the boussinesq approximation for liquids and gases. *Int. J. Heat Mass Transf.* **1976**, *19*, 545–551. [CrossRef]
27. The Hydrogen Data E Sharing Site. Available online: http://www.h2protocol.com/h2-fueling-data (accessed on 18 May 2020).
28. Dang, T.; Teng, J.-T. The effects of configurations on the performance of microchannel counter-flow heat exchangers—An experimental study. *Appl. Therm. Eng.* **2011**, *31*, 3946–3955. [CrossRef]
29. Dang, T.; Teng, J.-T.; Chu, J.-C. A study on the simulation and experiment of a microchannel counter-flow heat exchanger. *Appl. Therm. Eng.* **2010**, *30*, 2163–2172. [CrossRef]
30. Bahiraei, M.; Naseri, M.; Monavari, A. A CFD study on thermohydraulic characteristics of a nanofluid in a shell-and-tube heat exchanger fitted with new unilateral ladder type helical baffles. *Int. Commun. Heat Mass Transf.* **2021**, *124*, 105248. [CrossRef]
31. Zhang, J.-F.; Guo, S.-L.; Li, Z.-Z.; Wang, J.-P.; He, Y.-L.; Tao, W.-Q. Experimental performance comparison of shell-and-tube oil coolers with overlapped helical baffles and segmental baffles. *Appl. Therm. Eng.* **2013**, *58*, 336–343. [CrossRef]